Solar Energy Materials & Solar Cells 114 (2013) 147–155

Contents lists available at SciVerse ScienceDirect

Solar Energy Materials & Solar Cells

journal homepage: www.elsevier.com/locate/solmat

New progress in the fabrication of n–i–p micromorph solar cells for opaque substrates

Rémi Biron [a,*], Simon Hänni [a], Mathieu Boccard [a], Céline Pahud [a], Karin Söderström [a], Martial Duchamp [b], Rafal Dunin-Borkowski [b], Grégory Bugnon [a], Laura Ding [a], Sylvain Nicolay [a], Gaetano Parascandolo [a], Fanny Meillaud [a], Matthieu Despeisse [a], Franz-Josef Haug [a], Christophe Ballif [a]

[a] Ecole Polytechnique Fédérale de Lausanne (EPFL), Institute of Microengineering (IMT), Photovoltaics and Thin-Film Electronics Laboratory, 2000 Neuchâtel, Switzerland
[b] Institute for Microstructure Research, Ernst Ruska-Centre for Microscopy and Spectroscopy with Electrons Peter Gruenberg, Institute Research Centre Juelich, D-52425 Juelich, Germany

ARTICLE INFO

Article history:
Received 4 February 2013
Received in revised form
27 February 2013
Accepted 28 February 2013

Keywords:
Thin film silicon solar cells
Micromorph
Light trapping
Back reflector
Intermediate reflector

ABSTRACT

In this paper, we investigate tandem amorphous/microcrystalline silicon solar cells with asymmetric intermediate reflectors grown in the n–i–p substrate configuration. We compare different types of substrates with respect to their light-trapping properties as well as their influence on the growth of single-junction microcrystalline cells. Our most promising back reflector combines a textured zinc oxide film grown by low-pressure chemical vapor deposition, a silver film for reflection, and a zinc oxide buffer layer. Grown on this substrate, microcrystalline cells exhibit excellent response in the infrared while keeping high open-circuit voltage and fill factor, leading to efficiencies of up to 10.0%. After optimizing the morphology of the asymmetric intermediate reflector, we achieve an n–i–p micromorph solar cell stabilized efficiency of 11.6%, using 270 nm and 1.7 μm of silicon for the absorber layer of the amorphous top cell and the microcrystalline bottom cell, respectively. Using this original device architecture, we reach efficiencies close to those of state-of-the-art n–i–p and p–i–n micromorph devices, demonstrating a promising route to deposit high-efficiency thin-film silicon solar cells on opaque substrates.

1. Introduction

Thin-film silicon solar cells have the potential to reach lower production costs (€/W) than crystalline silicon cells thanks to the low material usage and reduced number of process steps inherent to thin-film technologies. Still, their efficiency should be further pushed to the limit. For instance, with respect to state-of-the-art crystalline silicon modules, the lower module efficiency of thin-film devices means more modules must be installed for a similar power, increasing the balance-of-systems cost. The micromorph technology, which combines amorphous (a-Si:H) and microcrystalline (μc-Si:H) silicon for the top and bottom cells, respectively, is in that regard a promising approach. Indeed this architecture has recently demonstrated laboratory cell efficiencies above 14% [1,2] and 12.3% [3,4] in the initial and stabilized states, respectively. At the same time, many groups have successfully developed various plasma-enhanced chemical vapor deposition (PE-CVD) processes to fabricate high-quality μc-Si:H bottom cells at high deposition rates above 1 nm/s [5–7]. As they have lower absorption coefficient in the NIR than other materials used as absorber layer in solar cells, a-Si:H and μc-Si:H layers necessitate light trapping to enhance the light path in the absorber layers, improving the probability that NIR photons will be absorbed and converted into electron–hole pairs. The desired light trapping can be achieved either via plasmonic effects [8–10] or via light scattering with random [11–13] and periodic [14–16] structures. Owing to its deposition sequence, the n–i–p configuration opens the route for direct depositions on opaque substrates like commercial ceramic tiles [17], flexible stainless steel [18,19] and plastic foils [20–22]. An additional advantage is that a large choice of light-scattering patterns covered with a silver (Ag) layer can be used to optimize light trapping in the bottom cell. Alternatively transparent conductive oxides (TCOs) with low free-carrier absorption can be combined with a Ag layer. Both options offer the possibility to increase the short-circuit current density (J_{sc}) of the bottom cell, leading to thinner silicon layers.

However, the required usage of textured electrodes leads to the formation of structural defects during the growth of the μc-Si:H cell, leading to lower electrical performance [23–25]. This detrimental effect can be mitigated by tuning the deposition

* Corresponding author. Tel.: +41 327183219.
E-mail address: remi.biron@epfl.ch (R. Biron).

0927-0248/$ - see front matter © 2013 Elsevier B.V. All rights reserved.
http://dx.doi.org/10.1016/j.solmat.2013.02.032

process parameters even at high deposition rates [26] and incorporating silicon oxide doped layers [27–29]. Another issue related to the use of patterned substrates is the self-texturing of the μc-Si:H film during PE-CVD, resulting in the formation of pinch points that form because of the change of the surface morphology of the silicon layer during its growth. The pinch points induce weak electrical performance in the subsequent top cell, decreasing the fill factor (FF) and the open-circuit voltage (V_{oc}) of tandem devices as reported in our recent work [30]. In the latter contribution, we reduced the detrimental effect of the pinch points by applying a low-pressure chemical vapor deposited zinc oxide (LP-CVD ZnO) layer which forms an excellent template for the top-cell growth after being subjected to a plasma treatment. Furthermore the LP-CVD ZnO layer serves as an asymmetric intermediate reflector (AIR) to reflect the light into the top cell, increasing its J_{sc} [31,32].

In Section 3.1, we show how we can mitigate the formation of porous defective areas in μc-Si:H single-junction solar cells by depositing an Ag layer at elevated temperature on the plasma-etched LP-CVD ZnO. This Ag layer smoothens the valleys of the plasma-etched LP-CVD ZnO texture and improves cell electrical performance compared to cells deposited on our standard LP-CVD ZnO textures. It also provides a good NIR response suitable for high J_{sc} in the bottom cell, which is our purpose to improve high-efficiency micromorph devices. In addition to the substrate fabricated in Section 3.1, in Section 3.2, we successfully develop another innovative substrate which offers better light trapping in the NIR and maintains high V_{oc} and FF values compared to Ag layer deposited at elevated temperature (HotAg) and our standard LP-CVD ZnO substrates. Then in Section 3.3, we optimize the AIR roughness by applying a newly developed pure oxygen (O_2) plasma treatment on its surface. Finally, in Section 3.4, we combine the best substrates developed in Sections 3.1 and 3.2 with the optimized AIR roughnesses into micromorph devices. With this novel architecture, we obtain highest initial and stabilized efficiencies of 13.2% and 11.6%, respectively, for n–i–p micromorph devices.

2. Experimental details

Fig. 1 shows the different substrates tested in single-junction μc-Si:H cells on glass. Type 1 refers to a 200-nm-thick Ag layer deposited by sputtering at 200 °C (Ag200), which is subsequently covered by 60 nm of sputtered aluminum-doped ZnO (ZnO:Al). Type 2 consists of 5-μm-thick LP-CVD ZnO etched for 45′ (Z5-45). Type 3 is made of 200-nm-thick flat Ag sputtered at room temperature (AgRT), which was subsequently covered by 60 nm of sputtered ZnO:Al. Afterwards, a non-intentionally-doped Z5 layer etched for 50′ (Z5-50 NID) is deposited on the stack. This structure has the advantages of high conductivity in the Ag film, adequate texture and low free-carrier absorption in the Z5-50 NID layer, and excellent scattering of NIR light. Type 4 consists of a Z5-45 layer covered by a 400-nm-thick silver layer deposited either at room temperature (AgRT) or at 150 °C (Ag150), corresponding to Type 4a and 4b substrates, respectively, which is subsequently covered by 60 nm of sputtered ZnO:Al.

The silicon films were deposited at temperatures ranging from 180 to 200 °C using PE-CVD. Since we used different deposition systems, further details on the deposition conditions are given in the text. On all cells, the front contact is made of an LP-CVD ZnO layer with half the thickness of Z5, i.e. 2.5 μm (Z5/2).

Micromorph devices were grown on Type 2, 3 and 4b substrates. The cell on the later substrate is showed in Fig. 1. The AIR layers were made of a non-intentionally-doped LP-CVD ZnO layer with a thickness of 1.1 μm. The thickness of the absorber layer of the a-Si:H top cell ranged from 220 to 270 nm. Finally, on each substrate, 16 cells of 0.25 cm^2 were patterned by lift-off lithography and plasma dry etching. For cell characterization, we measured the current–voltage (I–V) characteristic under a simulated AM1.5 g spectrum (WACOM WXS-220 S-L2, AM1.5GMM) and V_{oc} and FF were calculated from the I–V measurement. We determined J_{sc} through external quantum efficiency (EQE) measurement. Variable-illumination measurements (VIMs) were performed with neutral-color filters under the AM1.5 g spectrum. Initial efficiencies were measured after patterning of the cells. Stabilized efficiencies were measured after degradation for 1000 h at 50 °C under AM1.5 g illumination. The crystalline volume fraction of the films was assessed by Raman spectroscopy at the p-side of the cell (p-side R_c) using 514.5 nm light. We characterized the substrate morphology before cell deposition by atomic force microscopy (AFM) from which we extracted the root-mean-square roughness (σ_{rms}), correlation length (L) and mean angle ($\langle\alpha\rangle$) [33,34]. σ_{rms} and L quantify the average vertical and lateral dimensions of the surface structures, respectively, while $\langle\alpha\rangle$ characterizes their average slope.

3. Results and discussion

3.1. Effect of the deposition temperature of the Ag back reflector on single-junction μc-Si:H solar cell performance

To reach high-efficiency micromorph solar cells, we need high J_{sc} in the bottom cell, which is achieved by enhancing light trapping of NIR wavelengths. In this section we target the fabrication of a substrate consisting of a highly reflective Ag layer deposited on LP-CVD ZnO whose texture was reported to provide efficient NIR light scattering [35]. The deposition conditions of the additional Ag layer must be considered because the Ag growth may be influenced by the LP-CVD ZnO texture underneath, detrimentally modifying the ZnO surface morphology that was designed to be suitable for good μc-Si:H growth. In order to find an appropriate combination, we studied the influence of the deposition temperature of the Ag layer grown on top of the ZnO textures, as represented by Type 4a and 4b in Fig. 1. Then we grew

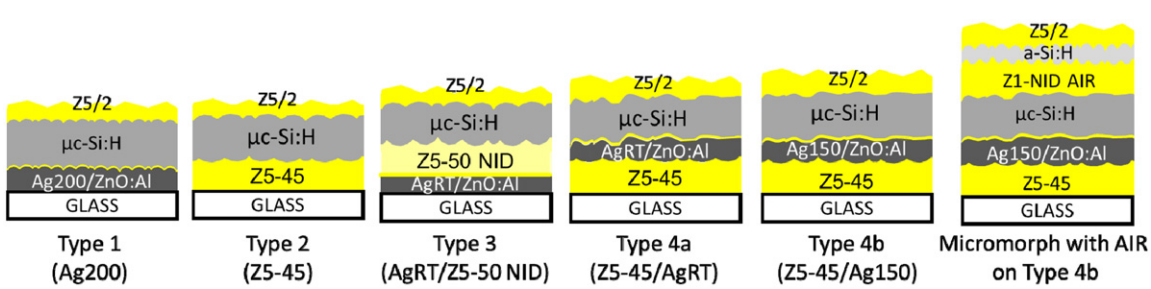

Fig. 1. Single-junction μc-Si:H cells with various substrate configurations. For the EQE measurement, white back reflectors are used at the rear of the Type 2 substrate. On the right, micromorph solar cell with an AIR deposited on 4b substrates.

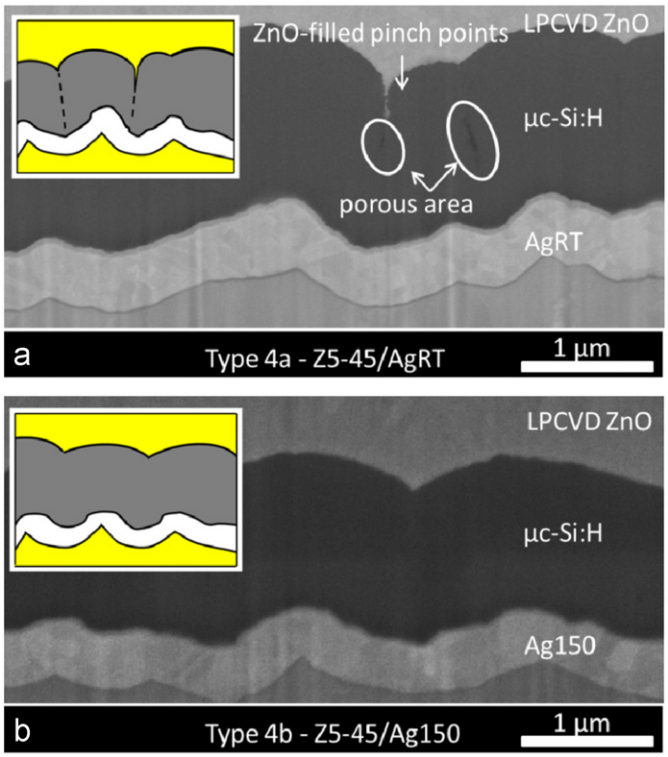

Fig. 2. SEM images of focused-ion-beam-prepared cross-sectional views of the 1.6-μm-thick μc-Si:H cells deposited on Type 4a (a) and 4b (b) substrates.

Table 1
Initial parameters of the co-deposited 1.6-μm-thick μc-Si:H cells with absorber layers deposited at VHF.

Substrate	p-side R_c [%]	V_{oc} [V]	FF [%]	J_{sc} [mA cm^{-2}]	η [%]
Type 4a (Z5-45/AgRT)	74	0.489	62.1	25.4	7.69
Type 4b (Z5-45/Ag150)	73	0.501	66.1	25.9	8.55

1.6-μm-thick μc-Si:H cells on these substrates. Cells were deposited at very high frequency (VHF) in a PE-CVD cluster tool (Octopus I, INDEOTec SA).

For Type 4a, the AgRT layer grows conformally on top of the plasma-etched LP-CVD ZnO pyramids, sharpening the valleys as illustrated in the scanning electron microscope (SEM) images in Fig. 2. It thus leads to the formation of structural defects in the μc-Si:H layer which are indicated in Fig. 2. In addition, deep pinch points appear at the top surface of the μc-Si:H layer which are filled afterward by the LP-CVD ZnO front contact. For these reasons, these cells exhibit lower FF and V_{oc} compared to cells on Type 4b substrates as shown in Table 1. Indeed, this undesirable AgRT morphology is avoided with the deposition of Ag150 as illustrated in Fig. 2. Ag150 films appear to be non-conformal, filling the valleys and smoothening the surface morphology, which seems to prevent the formation of structural defects. This is consistent with the observation of Söderström et al. for HotAg films deposited on thinner plasma-etched LP-CVD ZnO textures, as discussed in [36]. In this paper, valley filling was attributed to the self-texturing of the HotAg film which develops larger grains compared to AgRT films. Similar observations are made for Ag150 films used in this paper. The implementation of Ag150 films thus ameliorates the pinching problem while maintaining high J_{sc}, leading to a highest efficiency of 8.55% as shown in Table 1.

We suspect that the detrimental effect of Type 4a substrates is due to the sharpening of the valleys when the AgRT layer is deposited. This effect is expected to amplify with increasing AgRT layer thickness but could be mitigated by depositing thinner AgRT layers, e.g. 200 nm thick, which would also be more suitable for industrial applications. Nevertheless, we did not look into this issue and we will continue our investigation with Type 4b substrates.

3.2. Optimization of the substrate design for single-junction μc-Si:H cells with superior NIR response and electrical properties

3.2.1. Substrate design assessment at full illumination

In this section, the aim is to identify the substrate design that provides the best compromise between efficient NIR light trapping and optimum electrical properties for μc-Si:H cells in order to fabricate high-efficiency micromorph devices. In the previous section, we established that Type 4b substrates lead to a smoothened surface morphology, reducing the structural defect and pinching point density in the absorber layer compared to Type 4a substrates. Thus we compare Type 4b with Type 1, 2 and 3 substrates which exhibit very different surface morphologies as shown in Fig. 3 and Table 2. Based on the AFM measurements of Fig. 3, Type 1 substrates are smoother than the other substrates, presenting σ_{rms} and L of 29 and 165 nm, respectively, as listed in Table 2. These values are very similar to those of the HotAg films used by Unisolar [11]. Type 2 substrates have larger σ_{rms} and L values because of their large ZnO pyramids. The surface morphology of Type 3 substrates is even rougher since dopant-free ZnO deposition leads to the growth of bigger grains, resulting in larger pyramid sizes [13]. Finally, the surface roughness of Type 4b substrates is lower than Type 2, thanks to the Ag150 layer, which is consistent with the observations of the previous section.

In order to assess the potential of the substrates in micromorph devices, we first tested them in single-junction μc-Si:H cells. We deposited an absorber layer with a thickness of 1.7 μm using deposition processes which enable the improvement of the cell resilience to the substrate morphology [26,29]. The electrical performance of cells shown in Fig. 4 is higher for Type 1 substrates since these substrates are smoother than the other substrate types. We ascribe this trend to the high-quality growth of the silicon layers on small features, limiting the formation of structural defects within the absorber layer. Nevertheless, J_{sc} is significantly reduced and is attributed to weaker light trapping in the NIR region as shown by the EQE spectra in Fig. 5. Cells on Type 2 substrates are affected by lower FF and V_{oc}, probably due to the combination of the lower conductivity of the Z5-45 back contact compared to Ag, and an absorber layer of lower electronic quality, which appears to be not affected by structural defects since we did not observe them in SEM images of cross sections (not shown). Contrary to Type 2 substrates, Type 3 and 4b substrates have the advantage of maintaining electrical properties that are relatively similar to Type 1 while boosting the NIR response. In all cases, the EQE spectra exhibit a low response in the blue region since we did not optimize the transparency or thickness of the p-layer. Better performance for short wavelengths can be expected in micromorph devices since the p-layer of the a-Si:H top cell was designed to optimize the blue response. Nevertheless, as a result, the overall efficiency is successfully conserved at about 10% for Type 3 and 4b substrates while offering the possibility of bottom-cell J_{sc} of about 12.5 mA cm^{-2} in micromorph devices.

3.2.2. Substrate design assessment at reduced illumination

After assessing the light-trapping potential of the substrates at full illumination, we performed VIM for the best single-junction cell on each substrate. VIM evaluates the V_{oc} drop when a cell

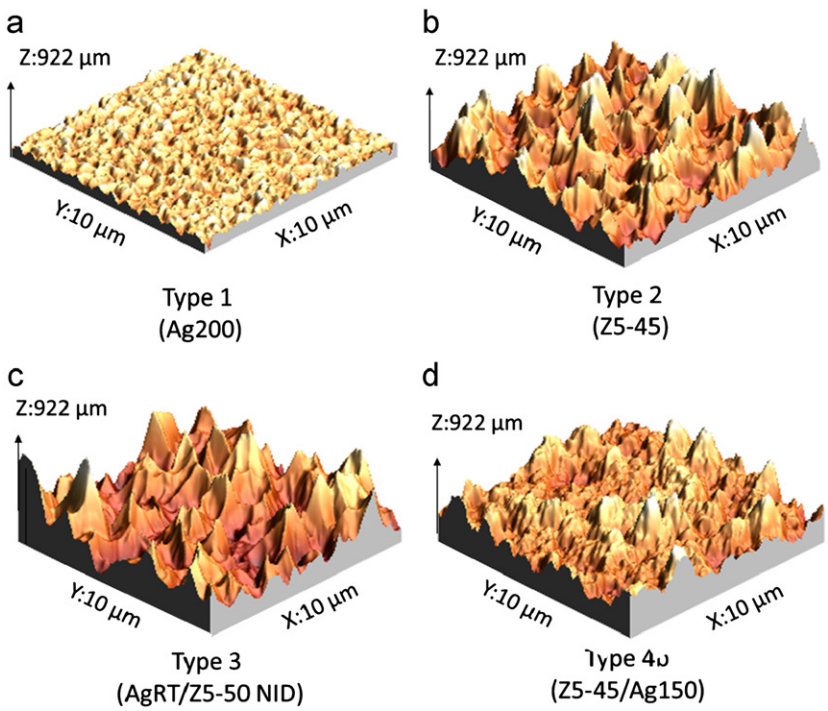

Fig. 3. 10 µm × 10 µm AFM images of the different substrates. As indicated in the figure, the *z*-scale is different between the images.

Table 2
Parameters of the surface morphology for the studied substrates extracted from the quantitative AFM analysis.

substrate	σ_{rms} [nm]	$\langle\alpha\rangle$ [deg]	L [nm]
Type 1 (Ag200)	29	21.9	165
Type 2 (Z5-45)	116	25.1	425
Type 3 (AgRT/Z5-50 NID)	151	25.5	535
Type 4b (Z5-45/Ag150)	102	26.3	484

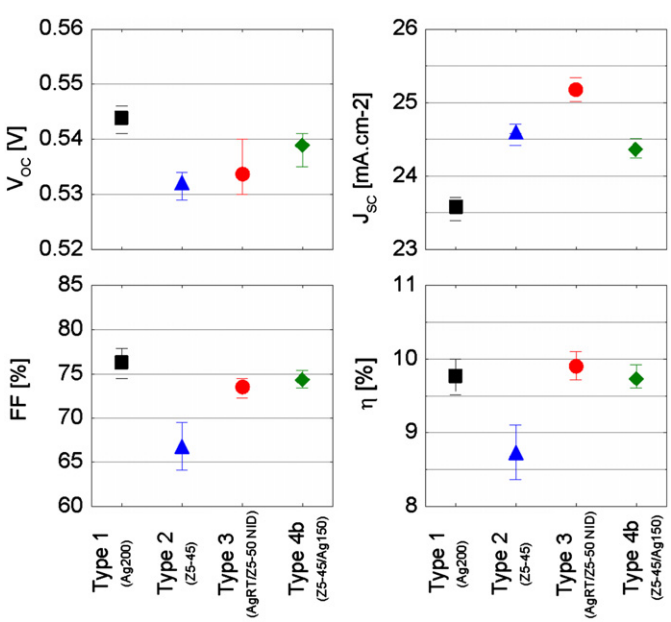

Fig. 4. Electrical parameters of 1.7-µm-thick single-junction µc-Si:H solar cells deposited on four different substrate types. The five best cells on each substrate were taken for the statistics; squares display the average value, and error bars correspond to the maximum and minimum values.

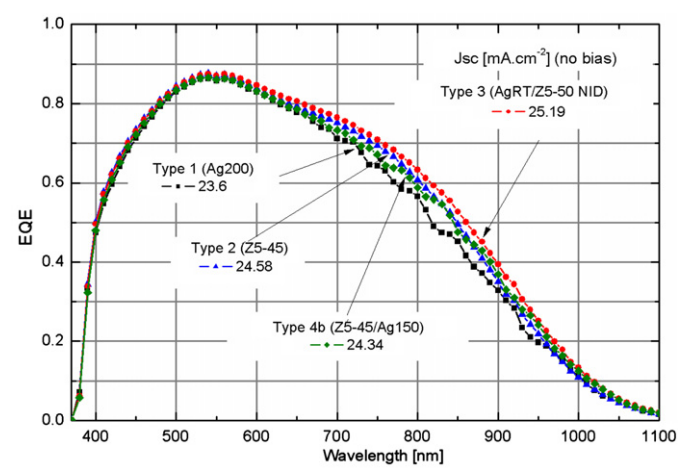

Fig. 5. EQE spectra of 1.7-µm-thick single-junction µc-Si:H best cells deposited on Type 1, 2, 3 and 4b substrates.

absorbs a smaller amount of light, as is the case in tandem cells. We attribute a higher V_{oc} drop to defective regions within the absorber layer in agreement with our previous observations [25,27]. We can thus determine which substrate will maintain the highest V_{oc} when incorporated into a micromorph cell. We deduced the diode quality factor n, by fitting the slope of the curves in Fig. 6 with the following one-diode model:

$$V_{oc} = nkT/q \ln(J_{sc}/J_0) \quad (1)$$

where T is the temperature in Kelvin, q the elementary charge, J_0 the saturation current, and k the Planck constant. Among substrates that provide high photocurrent, i.e. Type 2, 3 and 4b, cells grown on Type 4b substrates result in better V_{oc} than those on Type 2 and 3 substrates. Overall, the best absolute V_{oc} values as well as the smallest n values are observed for cells deposited on Type 1 substrates, as expected from the smoother morphology. We thus use this cell as a reference for the estimation of the

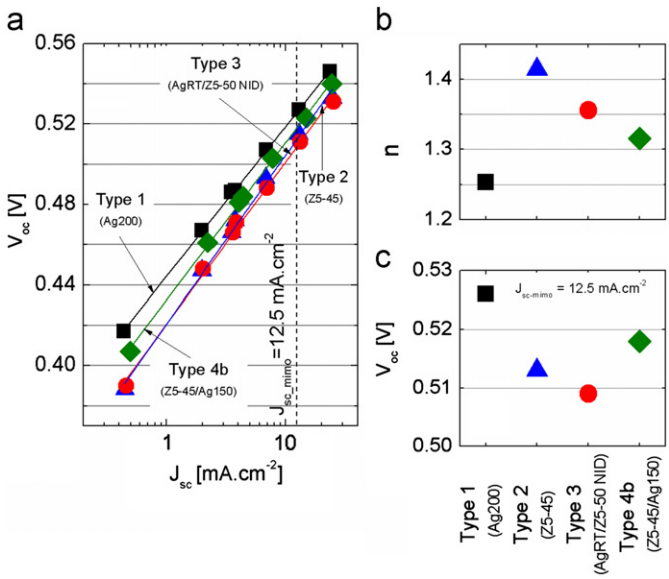

Fig. 6. (a) VIM of the best cells of each substrate. Full lines represent fits with Eq. (1) for each set of measurements. (b) The n values are deduced from Eq. (1), quantifying the V_{oc} drop with decreasing illumination. (c) The calculated V_{oc} values in the case of a bottom-cell J_{sc} of 12.5 mA cm^{-2} are shown in the bottom right from the data fitting.

V_{oc} losses in the micromorph cells deposited on the other substrates. Assuming a matched current of 12.5 mA cm^{-2}, from Fig. 6 (left), we can expect a bottom-cell V_{oc} of 526 mV. Compared to this upper limit, we anticipate V_{oc} losses linked to the illumination reduction of 13, 17 and 8 mV for cells on Type 2, 3 and 4b substrates, respectively. Nevertheless these substrates are more promising for obtaining micromorph cells of high efficiencies since we expect that V_{oc} losses will be easily balanced by higher J_{sc}, as these substrates provide better NIR light trapping compared to Type 1.

Based on these results, we chose Type 2, 3 and 4b substrates as the best candidates for the realization of record micromorph devices since they offer a better compromise between satisfactory NIR response and V_{oc} and FF values for an absorber layer thickness of 1.7 μm compared to Type 1 substrates. In the following section, we incorporate Type 2 substrates as back electrodes into micromorph cells for optimization of the AIR morphology.

3.3. Effect of AIR roughness on micromorph cell performance

Light trapping in the top cell is of equal importance to light trapping in the bottom cell, but their optimization aims for different targets, as high J_{sc} in the top cell must be achieved with a thin a-Si:H absorber layer because light-induced degradation increases with a-Si:H layer thickness [37,38]. We further seek to fabricate a bottom-limited device since such devices typically exhibit higher FF compared to top-limited devices because of the higher electronic quality of the μc-Si:H intrinsic material [39,40].

Therefore, we introduce an AIR that consists of a 1.1-μm-thick NID LP-CVD ZnO layer to enhance the top-cell J_{sc} as previously reported by Söderström et al. [29] and Bugnon et al. [30] in the n–i–p and p–i–n configurations, respectively. We change the roughness of the AIR by applying a pure O_2 plasma treatment which increases the lateral resistivity of the layer without compromising the out-of-plane conductivity. For the lateral resistivity, we measure an increase of sheet resistance from several hundreds to mega ohms. This mitigates current drains that may occur in both sub-cells, thus leading to higher micromorph V_{oc} [28]. The plasma treatment also transforms the V-shaped valleys into U-shaped valleys as reported by Bailat et al. [41]. As a result the roughness of the AIR decreases as the plasma treatment time increases from 15′ to 60′, leading to further increased V_{oc} and FF of micromorph cells in both the initial and stabilized states as displayed in Fig. 7. Independently, the J_{sc} gain in the top cell for rougher AIRs is compensated by a strong drop in V_{oc} and FF. We explain this sharp decrease by the fact that, with our deposition processes for a-Si:H top cells, the AIR roughness has to be below 50 nm to maintain good electrical properties of tandem devices, as recently reported [42].

The highest stabilized efficiency of 11.1% is obtained for the smoothest AIR as it maintains the highest V_{oc} and FF upon degradation. However the smoothest AIR leads to a strongly top-limited device because of the low scattering at the AIR/top-cell interface.

3.4. Interdependence of the substrate and AIR roughnesses on micromorph cell performance

As a last step to further optimize the full micromorph device, we focus on the interplay between the substrate and AIR roughnesses. We increased as next step the absorber layer thicknesses of the top and bottom cells to 270 nm and 1.7 μm, respectively, to obtain a high current-matching value of 12.5 mA cm^{-2}. The bottom cells were co-deposited with the cells shown in Section 3.2. We also used long-duration pure O_2 plasma treatments, i.e. 30′ (rough) and 60′ (smooth), for AIR roughness optimization to maintain high-performance devices, as demonstrated in the previous section. Fig. 8 shows cell parameters in both the initial and stabilized states as a function of the substrate type and AIR plasma treatment.

In the initial state, V_{oc} decreases for cells on rougher AIRs as already observed in Fig. 7, independent of the substrate type. Furthermore, the V_{oc} difference between micromorph cells on smooth and rough AIRs is lower than the expected V_{oc} loss in bottom cells calculated in Section 3.2, confirming that the top-cell V_{oc} also strongly affects the micromorph V_{oc}. The V_{oc} dependence on AIR roughness is also apparent in the stabilized state, except for cells on Type 3 substrates. After degradation, V_{oc} remains above the high value of 1.40 V. FF increases artificially with the current mismatching and, as expected, FF is higher for bottom-limited devices like the cells on Type 4b substrates with rougher AIRs. The best stabilized efficiency of 11.6% is obtained with these cells. This is close to state-of-the-art efficiencies, as reported by Unisolar [43,44], and to some extent 1 cm^2 p–i–n cells developed in-house [45]. The EQE spectra of the best cell on a Type 4b substrate as well the cross section of the cell are displayed in Fig. 9.

Stabilized efficiencies of 11.2% and 11.4% were obtained for Type 2 and 3 substrates, respectively, but with more statistical scatter among the 16 tested cells. Interestingly, we found that the total J_{sc} of cells on Type 3 substrates was from 0.6 to 1.1 mA cm^{-2} higher compared to micromorph cells deposited on other substrates. We attribute this gain to a better interplay between Type 3 substrates and the AIR morphology in increasing NIR light trapping.

4. Outlook

Because most of the cells shown in the previous section are top limited, it should be possible to obtain similar efficiencies with thinner bottom cells for cells with smooth AIRs. According to our experience when depositing single-junction μc-Si:H cells on Type 2 substrates [42], a smaller absorber layer thickness of 1.3–1.4 μm for the bottom cell can be sufficient to match both

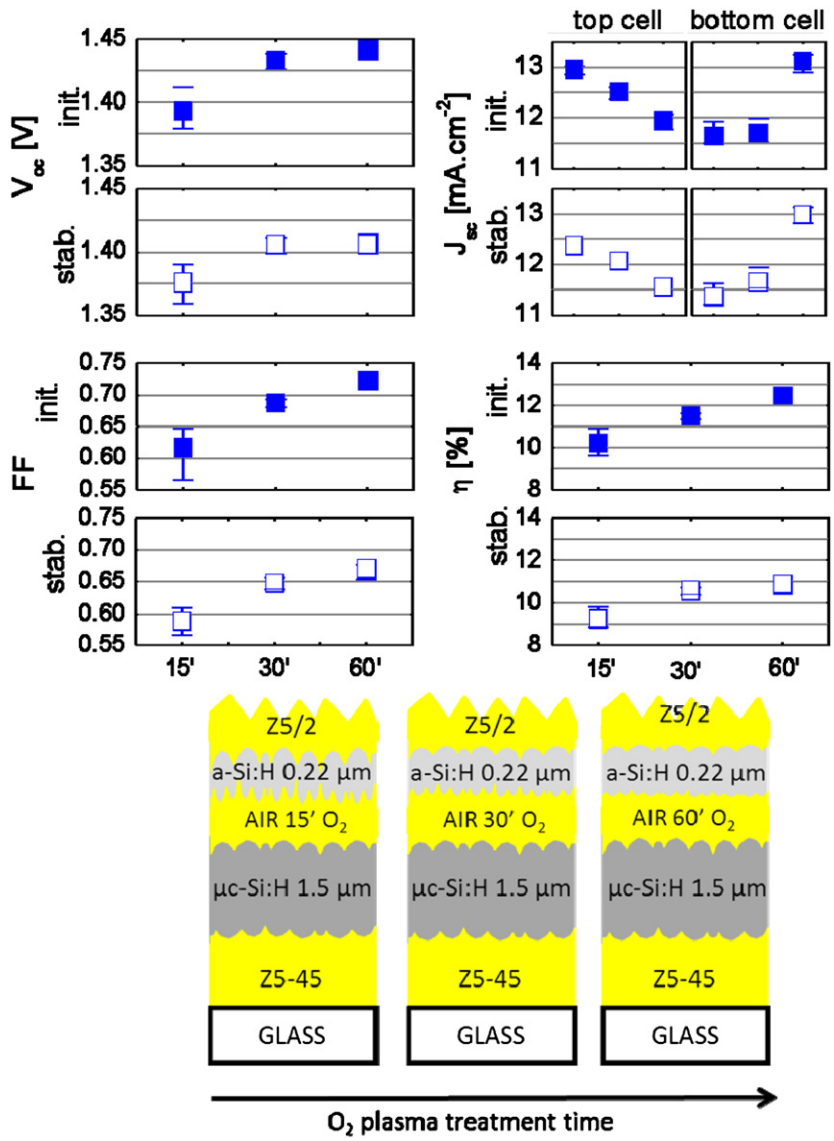

Fig. 7. Electrical performance of the five best micromorph cells deposited on Type 2 substrates with O_2 plasma treatment times of 15′, 30′ and 60′ in the initial and stabilized states. Squares display the average value, and error bars correspond to the maximum and minimum values. The absorber layer thicknesses of the top and bottom cells are 220 nm and 1.5 µm, respectively.

sub-cells at J_{sc} values equal to those of micromorph cells with smooth AIRs.

For cells with rough AIRs, provided that we conserve the top-cell thickness, we reach the highest possible efficiency on Type 2 substrates since the sub-cells are matched. On the contrary, the use of Type 3 substrates is beneficial since higher stabilized efficiencies are obtained. In addition, similar efficiencies can be achieved by reducing the absorber layer thickness of the bottom cell by 0.3 to 0.5 µm based on our previous results on Type 2 substrates [42]. Finally, this substrate opens the route to match sub-cells at higher J_{sc} values while keeping identical bottom-cell thicknesses.

The highest efficiencies are obtained with Type 4b substrates because of the better V_{oc} and FF values. Even higher efficiencies could be projected if the sub-cell J_{sc} was matched at 12.5 mA cm^{-2} with a slightly thicker bottom cell. The other advantage of depositing a Ag layer at the top of the texture is that we can easily incorporate any type of texture via the potentially low-cost nano-imprinting process [46–49], permitting the deposition of thinner devices. For example, we could easily incorporate a nano-imprinted replica of plasma-etched LP-CVD ZnO or the honeycomb patterns on which Sai et al. reported J_{sc} above 26 mA cm^{-2} for 1-µm-thick single-junction µc-Si:H cells [50]. Since both Type 3 and 4b substrates offer the possibility to deposit thinner bottom cells which usually exhibit higher V_{oc} and FF, we can expect better electrical performance for tandem devices.

Another way to achieve higher efficiencies is to enhance the top-cell J_{sc} which is revealed to be the limiting parameter for the majority of cells, even for those with rougher AIRs. Top-cell J_{sc} saturates at 12.5 mA cm^{-2} for a 270-nm-thick absorber layer which is already significantly affected by light-induced degradation. The use of an intermediate reflector material with a lower refractive index than ZnO like magnesium fluoride is a promising option as suggested by Krc et al. [51], but it has not yet been implemented into devices.

Alternatively, the a-Si:H/µc-Si:H/µc-Si:H triple-junction cell is a promising option to improve efficiency owing to its lower degradation. This configuration has demonstrated stabilized efficiencies above 13% and 12.5% on relatively smooth HotAg [52] and physically flat/optically rough substrates [53,54], respectively, which enable the growth of high-electronic-quality silicon layers, leading to high V_{oc} and FF values. As they are deposited on

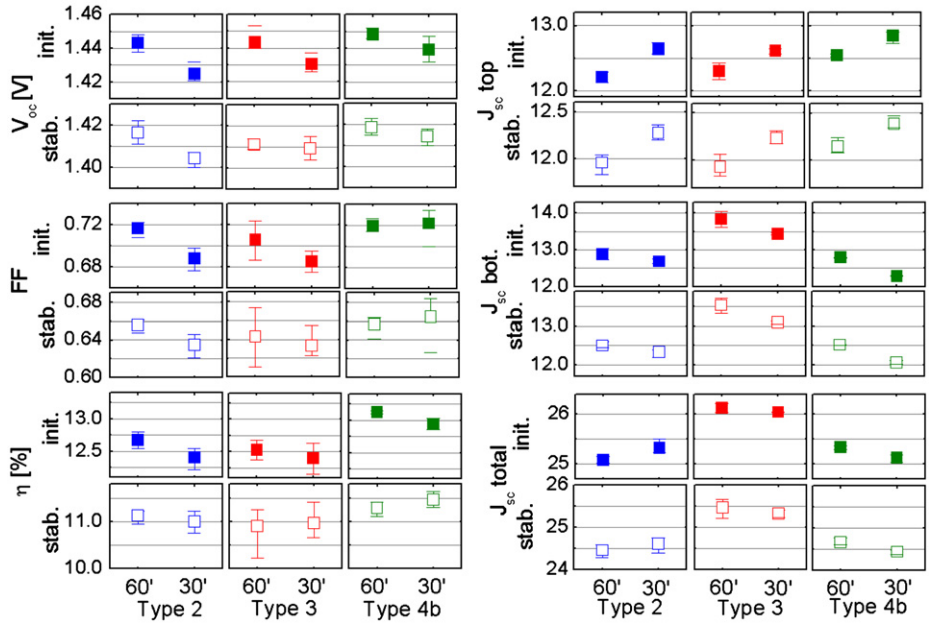

Fig. 8. Initial and stabilized cell parameters of micromorph devices as a function of substrate type and AIR roughness. The five best cells on each substrate were taken for the statistics; squares display the average value, and error bars correspond to the maximum and minimum values.

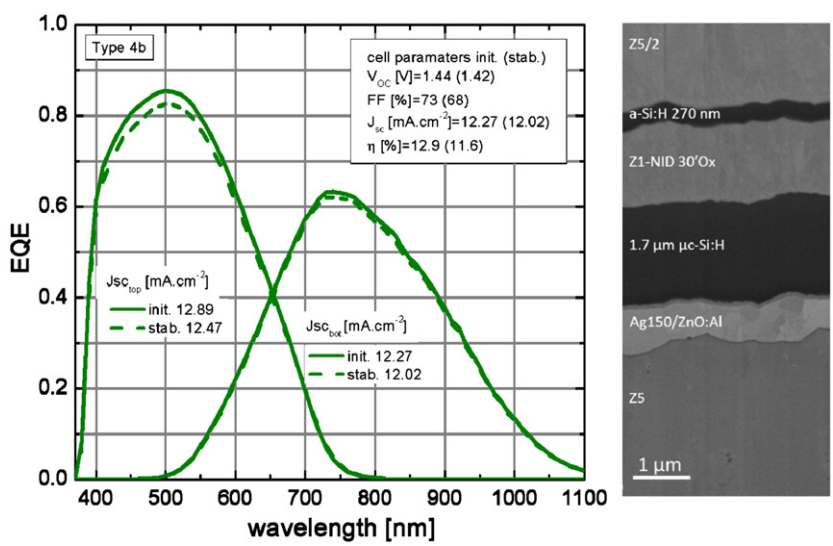

Fig. 9. EQE of the best stabilized micromorph cell deposited on a Type 4b substrate. Cell parameters in both the initial and stabilized states are given in the inset. On the right, SEM images of focused-ion-beam-prepared cross-sectional views of the cell.

smooth substrates, the µc-Si:H layers of triple junctions are relatively thick compared to those in micromorph devices deposited on rough electrodes. The challenge is thus the deposition of triple-junction cells on rougher substrates. Type 3 and 4b substrates demonstrate good light scattering in the NIR which could be suitable for triple-junction applications. In addition, an AIR layer grown on textured electrodes that flattens pinch points at the top surface of the bottom cell can offer an optimal morphology for deposition of the middle and top cells, resulting in high V_{oc} and FF values.

5. Conclusion

We demonstrated that an optimum trade-off is found between high optical and electronic properties of both sub-cells in n–i–p micromorph devices with AIRs. This novel micromorph architecture offers the possibility to tune the growth interface of the top cell regardless of the bottom-cell texture while having high-electronic-quality silicon layers via the use of adjustable texture of the back electrode thanks to a highly reflective and conductive Ag layer and an adaptable AIR morphology. The experiments carried out on micromorph cells with various combinations of substrate and intermediate reflector textures show that it is difficult to combine high V_{oc} and FF with high J_{sc} for both sub-cells. Nevertheless, it is possible that a good balance can be found with $V_{oc} > 1.4$ V and total $J_{sc} \sim 25$ mA cm^{-2} for a stabilized efficiency of 11.6%.

Acknowledgments

The authors acknowledge the support of the EU-Project Si-Light (Contract No. 241277) and the Swiss Federal Energy Office (Contract No. SI/500750-01).

References

[1] M. Boccard, C. Battaglia, S. Hänni, K. Söderström, J. Escarré, S. Nicolay, F. Meillaud, M. Despeisse, C. Ballif, Multiscale transparent electrode architecture for efficient light management and carrier collection in solar cells, Nano Letters 12 (2012) 1344–1348.

[2] K. Yamamoto, A. Nakajima, M. Yoshimi, T. Sawada, S. Fukuda, T. Suezaki, M. Ichikawa, Y. Koi, M. Goto, T. Meguro, T. Matsuda, M. Kondo, T. Sasaki, Y. Tawada, A high efficiency thin film silicon solar cell and module, Solar Energy 77 (2004) 939–949.

[3] M.A. Green, K. Emery, Y. Hishikawa, W. Warta, E.D. Dunlop, Solar Cell Efficiency Tables (version 41)Progress in Photovoltaics: Research and Applications 21 (2013) 1–11.

[4] U. Kroll, J. Meier, L. Fesquet, J. Steinhauser, S. Benagli, J.-B. Orhan, B. Wolf, D. Borrello, L. Castens, Y. Djeridane, X. Multone, G. Choong, D. Domine, J.-F. Boucher, P.-A. Madliger, M. Marmelo, G. Monteduro, B..Dehbozorgi, D. Romang, E. Omnes, M. Chevalley, G. Charitat, A. Pomey, E. Vallat-Sauvain, S. Marjanovic, G. Kohnke, K. Koch, J. Liu, R. Modavis, D. Thelen, S. Vallon, A. Zakharian, D. Weidman, Recent developments of high-efficiency micromorph tandem solar cells in KAI-M/plasmabox PECVD reactors, in: Proceedings of the 26th PVSEC Hamburg, 2001, pp. 2340–2343.

[5] T. Matsui, A. Matsuda, M. Kondo, High-rate microcrystalline silicon deposition for p–i–n junction solar cells, Solar Energy Materials and Solar Cells 90 (2006) 3199–3204.

[6] M. Kondo M.T. Matsui T.Y. Nasuno, et al. Crucial processing steps for microcrystalline silicon bottom cells, in: Proceedings of the 31st IEEE Photovoltaic Specialists Conference, 2005, pp. 1377–1382.

[7] B. Yan G. Yue, J. Yang, K. Lord, A. Banerjee, S. Guha, Microcrystalline silicon solar cells made using RF, MVHF, and microwave at various deposition rates, in: Proceedings of the 3rd World Conference on Photovoltaic Energy Conversion Osaka Japan: Photovoltaic Science and Engineering Conference Committee, 2003, p. 2773.

[8] F.J. Beck, A. Polman, K.R. Catchpole, Tunable light trapping for solar cells using localized surface plasmons, Journal of Applied Physics 105.11 (2009)114310-114310.

[9] C. Eminian, F.-J. Haug, C. Garcia, O. Jesus, X. Niquille, C. Ballif, Photocurrent enhancement in thin film amorphous silicon solar cells with silver nanoparticles, Progress in Photovoltaics: Research and Applications 19 (2011) 260–265.

[10] H. Tan, R. Santbergen, A.H.M. Smets, M. Zeman, Plasmonic light trapping in thin-film silicon solar cells with improved self-assembled silver nanoparticles, Nano Letters 12 (8) (2012) 4070–4076.

[11] B. Yan, J.M. Owens, C.-S. Jiang, J. Yang, J.S. Guha, Improved back reflector for high efficiency hydrogenated amorphous and nanocrystalline silicon-based solar cells, Materials Research Society Symposium Proceedings 862 (2005) 603–608.

[12] J. Müllera, B. Rech, J. Springerb, M. Vanecekb, TCO and light trapping in silicon thin film solar cells, Solar Energy 77.6 (2004) 917–930.

[13] S. Faÿ, L. Feitknecht, R. Schlüchter, U. Kroll, E. Vallat-Sauvain, et al., Rough ZnO Layers by LP-CVD process and their effect in improving performances of amorphous and microcrystalline silicon solar cells, Solar Energy Materials and Solar Cells 90 (2006) 2960–2967.

[14] U.W. Paetzold, E. Moulin, D. Michaelis, W. Böttler, C. Wächter, V. Hagemann, M. Meier, R. Carius, U. Rau, Plasmonic reflection grating back contacts for microcrystalline silicon solar cells, Applied Physics Letters 99 (2011) 181105-1–181105-3.

[15] H. Sai, H. Fujiwara, M. Kondo, Back surface reflectors with periodic textures fabricated by self-ordering process for light trapping in thin-film microcrystalline silicon solar cells, Solar Energy Materials and Solar Cells93.6 (2009) 1087–1090.

[16] K. Söderström, F.-J. Haug, J. Escarre´, O. Cubero, C. Ballif, Photocurrent increase in n–i–p thin film silicon solar cells by guided mode excitation via grating coupler, Applied Physics Letters 96 (2010) 213508-1–213508-3.

[17] H. Aguas, S.K. Ram, A. Ara_ujo, D. Gaspar, A. Vicente, S.A. Filonovich, E. Fortunato, R. Martins, I. Ferreira, Silicon thin film solar cells on commercial tiles, Energy & Environmental Science 4 (2011) 4620.

[18] B.B. Van Aken, J. Löffler, M.C.R. Heijna, W.J. Soppe, Inline deposited thin-film silicon solarcells on imprinted foil using linear PECVD sources, Journal of Non-Crystalline Solids 358 (2012) 2268–2271.

[19] B. Yan, J. Yang, S. Guha, Amorphous and nanocrystalline silicon thin film photovoltaic technology on flexible substrates, Journal of Vacuum Science and Technology A 30 (2012) 04D108.

[20] M.A. González Lazo, R. Teuscher, Y. Leterrier, J.-A.E. Månson, C. Calderone, A. Hessler-Wyser, P. Couty, Y. Ziegler, D. Fischer, UV-nano-imprint lithography and large area roll-to-roll texturization with hyperbranched polymer nanocomposites for light-trapping applications, Solar Energy Materials and Solar Cells 103 (2012) 147–156.

[21] H. Li, C.H.M. van der Werf, A. Borreman, J.K. Rath, R.E.I. Schropp, Flexible a-Si/μc-Si tandem thin film silicon solar cells on plastic substrates with i-layers made with hot-wire CVD using the Helianthos cell transfer process, in: Proceedings of the 33rd IEEE PVSC, 2008, pp. 1–6.

[22] Y. Ichikawa, T. Yoshida, T. Hama, H. Sakai, K. Harashima, Production technology for amorphous silicon-based flexible solar cells, Solar Energy Materials and Solar Cells 66 (2001) 107–115.

[23] Y. Nasuno, M. Kondo, A. Matsuda, Effect of substrate morphology on microcrystalline silicon solar cells, Japanese Journal of Applied Physics 40 (2011) 303–305.

[24] H.B.T. Li, R.H. Franken, J.K. Rath, R.E.I. Schropp, Structural defects caused by a rough substrate and their influence on the performance of hydrogenated nano crystalline silicon n–i–p solar cells, Solar Energy Materials and Solar Cells 93 (2009) 338–349.

[25] M. Python, E. Vallat-Sauvain, J. Bailat, D. Dominé, L. Fesquet, A. Shah, C. Ballif, Relation between substrate surface morphology and microcrystalline silicon solar cell performance, Journal of Non-Crystalline Solids 354 (2008) 2258–2262.

[26] G. Bugnon, G. Parascandolo, T. Söderström, P. Cuony, M. Despeisse, S. Hänni, J. Holovsky, F. Meillaud, C. Ballif, A new view of microcrystalline silicon: the role of plasma processing in achieving a dense and stable absorber material for photovoltaic applications, Advanced Functional Materials 22 (2012) 3665–3671.

[27] S. Hanni, D.T.L. Alexander, L. Ding, G. Bugnon, M. Boccard, C. Battaglia, P. Cuony, J. Escarré, G. Parascandolo, S. Nicolay, M. Cantoni, M. Despeisse, F. Meillaud, C. Ballif, On the interplay between microstructure and interfaces in high-efficiency microcrystalline silicon solar cells, IEEE Journal of Photovoltaics 3 (2012) 11–16.

[28] P. Cuony, M. Marending, D.T.L. Alexander, M. Boccard, G. Bugnon, M. Despeisse, C. Ballif, Mixed-phase p-type silicon oxide containing silicon nanocrystals and its role in thin-film silicon solar cells, Applied Physics Letters 97 (2010) 213502-1–213502-3.

[29] M. Despeisse, C. Battaglia, M. Boccard, G. Bugnon, M. Charrière, P. Cuony, S. Hänni, L. Löfgren, F. Meillaud, G. Parascandolo, T. Söderström, C. Ballif, Optimization of thin film silicon solar cells on highly textured substrates, Physica Status Solidi A 208 (2011) 1863–1868.

[30] R..Biron et al., in preparation.

[31] T. Söderström, F.-J. Haug, X. Niquille, V. Terrazzoni, C. Ballif, Asymmetric intermediate reflector for tandem micromorph thin film silicon solar cells, Applied Physics Letters 94 (2009) 063501-1–063501-3.

[32] G. Bugnon, T. Söderström, S. Nicolay, L. Ding, M. Despeisse, A. Hedler, J. Eberhardt, C. Wachtendorf, C. Ballif, LPCVD ZnO-based intermediate reflector for micromorph tandem solar cells, Solar Energy Materials and Solar Cells 95 (2010) 2161–2166.

[33] K. Söderström, J. Escarré, O. Cubero, F.-J. Haug, S. Perregaux, C. Ballif, UV-nano-imprint lithography technique for the replication of back reflectors for n–i–p thin film silicon solar cells, Progress in Photovoltaics: Research and Applications 19 (2011) 202–210.

[34] J. Escarré, C. Battaglia, K. Söderström, C. Pahud, R. Biron, O. Cubero, F.-J. Haug, C. Ballif, UV imprinting for thin film solar cell application, Journal of Optics 14 (2012) 024009 (8 pp.).

[35] S. Nicolay, S. Faÿ, C. Ballif, Growth model of MOCVD polycrystalline ZnO, Crystal Growth & Design 9 (2009) 4957–4962.

[36] K. Söderström, F.-J. Haug, J. Escarré, C. Pahud, R. Biron, C. Ballif, Highly reflective nanotextured sputtered silver back reflector for flexible high-efficiency n–i–p thin-film silicon solar cells, Solar Energy Materials and Solar Cells 95 (2011) 3585–3591.

[37] H. Sakai, T. Ihara, O. Nabeta, T. Yoshida, K. Maruyama, Y. Ichikawa, Y. Uchida, in: A. Madan, M. Thompson, D. Adler, Y. Hamakawa (Eds.), Materials Research Society Symposium Proceedings, vol. 95, Anaheim, MRS, Pittsburgh, 1987, p. 589.

[38] B. Rech, H. Wagner, Potential of amorphous silicon for solar cells, Applied Physics 69 (1999) 155–167.

[39] J. Burdick, T. Glatfelter, Spectral response and *I–V* measurement of tandem amorphous-silicon alloy solar cells, Solar Cells 18 (1986) 301–314.

[40] M. Bonnet-Eymard et al., Solar Energy Materials & Solar Cells, submitted for publication.

[41] J. Bailat, D. Dominé, R. Schlüchter, J. Steinhauser, S. Faÿ, F. Freitas, C. Bücher, L. Feitknecht, X. Niquille, T. Tscharner, A. Shah, C. Ballif, High-efficiency p–i–n microcrystalline and micromorph solar cells deposited on LPCVD ZnO coated glass substrates, in: Proceedings of the 4th World Conference Photovoltaic Energy Conversion, 2006, pp. 1533–1536.

[42] R. Biron, S. Hänni, M. Boccard, C. Pahud, G. Bugnon, L. Ding, S. Nicolay, G. Parascandolo, F. Meillaud, M. Despeisse, F.-J. Haug, C. Ballif, Optimization of the asymmetric intermediate reflector morphology for high stabilized efficiency thin n–i–p micromorph solar cells, IEEE Journal of Photovoltaics 3 (2012
) 41–45.

[43] J. Yang, S. Guha, Status and future perspective of a-Si:H, a-SiGe:H, and nc-Si:H thin film photovoltaic technology, Proceedings of SPIE 7409, 74090C (pp. 1–14).

[44] B. Yan, G. Yue, S. Guha, Status of nc-Si:H solar cells at United Solar and Roadmap for manufacturing a-Si:H and nc-Si:H based solar panels, Materials Research Society Symposium Proceedings 989 (2007).

[45] M. Despeisse, M. Boccard, C. Battaglia, M. Charrière, L. Garcia, M. Bonnet-Eymard, J..Escarre, P. Cuony, M..Stuckelberger, S. Hänni, L. Löfgren, Jan-Willem Schüttauf, L. Ding, S. Nicolay, F.Meillaud, C. Ballif , Light harvesting schemes for high efficiency thin film silicon solar cells, in: Proceedings of the 38th IEEE PVSC, 2012, pp. 003015–003019.

[46] J. Escarre, K. Söderström, C. Battaglia, F.-J. Haug, C. Ballif, High fidelity transfer of nanometric random textures by UV embossing for thin film solar cells applications, Solar Energy Materials and Solar Cells 95 (2011) 881–886.

[47] V.E. Ferry, M.A. Verschuuren2, H.B.T. Li, R.E.I. Schropp, H.A. Atwater, A. Polman, Improved red-response in thin film a-Si:H solar cells with soft-imprinted plasmonic back reflectors, Applied Physics Letters 95 (2009) 183503.

[48] U.W. Paetzold, W. Zhang, M. Prömpers, J. Kirchhoff, T. Merdzhanova, S. Michard, R. Carius, A. Gordijn, M. Meier, Thin-film silicon solar cell development on imprint-textured glass substrates, Materials Science and Engineering B, http://dx.doi.org/10.1016/j.mseb.2013.01.005, in press.

[49] A. Bessonov, Y. Cho, S.-J. Jung, E.-A. Park, E.-S. Hwang, J.-W. Lee, M. Shinb, S. Lee, Nanoimprint patterning for tunable light trapping in large-area silicon solar cells 95 (2011) 2886–2892Solar Energy Materials and Solar Cells 95 (2011) 2886–2892.

[50] H. Sai, K. Saito, M. Kondo, Enhanced photocurrent and conversion efficiency in thin-film microcrystalline silicon solar cells using periodically textured back reflectors with hexagonal dimple arrays, Applied Physics Letters 101 (2012) 173901.

[51] J. Krc, F. Smole, M. Topic, Advanced optical design of tandem micromorph silicon solar cells, Journal of Non-Crystalline Solids 352 (2006) 1892–1895.

[52] B. Yan, G. Yue, L. Sivec, J. Yang, S. Guha, C.-S. Jiang, Innovative dual function nc-SiO_x:H layer leading to a $>16\%$ efficient multi-junction thin-film silicon solar cell, Applied Physics Letters 99 (2011) 113512.

[53] K. Söderström, G. Bugnon, R. Biron, C. Pahud, F. Meillaud, F.-J. Haug, C. Ballif, Thin-film silicon triple-junction solar cell with 12.5% stable efficiency on innovative flat light scattering substrate, Journal of Applied Physics112 (2012) 114503.

[54] O. Isabella, H. Sai, M. Kondo, M. Zeman, Full-wave optoelectrical modeling of optimized flattened light-scattering substrate for high efficiency thin-film silicon solarcells, Progress in Photovoltaics: Research and Applications, http://dx.doi.org/10.1002/pip.2314, in press.